Inkjet Printing of Functional and Structural Materials: Fluid Property Requirements, Feature Stability, and Resolution

Brian Derby

Materials Science Center, School of Materials, University of Manchester, Manchester, M1 7HS, United Kingdom; email: brian.derby@manchester.ac.uk

Annu. Rev. Mater. Res. 2010. 40:395–414

First published online as a Review in Advance on March 9, 2010

The *Annual Review of Materials Research* is online at matsci.annualreviews.org

This article's doi: 10.1146/annurev-matsci-070909-104502

1531-7331/10/0804-0395$20.00

Key Words

contact angle, drop formation, surface energy, drying

Abstract

Inkjet printing is viewed as a versatile manufacturing tool for applications in materials fabrication in addition to its traditional role in graphics output and marking. The unifying feature in all these applications is the dispensing and precise positioning of very small volumes of fluid (1–100 picoliters) on a substrate before transformation to a solid. The application of inkjet printing to the fabrication of structures for structural or functional materials applications requires an understanding as to how the physical processes that operate during inkjet printing interact with the properties of the fluid precursors used. Here we review the current state of understanding of the mechanisms of drop formation and how this defines the fluid properties that are required for a given liquid to be printable. The interactions between individual drops and the substrate as well as between adjacent drops are important in defining the resolution and accuracy of printed objects. Pattern resolution is limited by the extent to which a liquid drop spreads on a substrate and how spreading changes with the overlap of adjacent drops to form continuous features. There are clearly defined upper and lower bounds to the width of a printed continuous line, which can be defined in terms of materials and process variables. Finer-resolution features can be achieved through appropriate patterning and structuring of the substrate prior to printing, which is essential if polymeric semiconducting devices are to be fabricated. Low advancing and receding contact angles promote printed line stability but are also more prone to solute segregation or "coffee staining" on drying.

INTRODUCTION

Inkjet printing as a distinct concept can be traced back to a patent granted to Lord William Kelvin, the nineteenth-century physicist and polymath, for the direction of droplets through electrostatic forces (1). However, without the means to generate detailed instructions to steer the droplets, inkjet printing remained unused until the 1950s, when Siemens used the technique to plot machine output traces. Major advances occurred in the period 1960–1980 to develop the technology for computer graphics output, with further advances in manufacturing technology and reductions in costs and size of the printers. Inkjet printing is now an ubiquitous personal printing tool. The main commercial application for inkjet printing remains in graphics and other conventional printing operations. However, in recent years there has been considerable interest in, and use of, inkjet printing as a fabrication tool in a number of areas of technology, including displays (2), plastic electronics (3), solder dispensing for flip-chip manufacture (either directly or as a solder mask) (4), rapid prototyping (5), ceramic component manufacture (6), enzyme-based sensors (7), and tissue engineering (8). Inkjet printing is currently at the threshold of becoming a standard fabrication tool, with a wide range of materials science applications (9, 10).

The application of inkjet printing to this disparate group of topics reflects the versatility of the method, which is the accurate positional placement of picoliter volumes of fluid on an arbitrary substrate. Although couched in rather simple terms, this definition encompasses a number of physical operations that both define and constrain inkjet printing. These are

1. generation of droplets,
2. positioning of and interaction of droplets on a substrate, and
3. drying or other solidification mechanisms to produce a solid deposit.

This review explores how these common features of the inkjet process interact with materials during the fabrication of structures by inkjet printing.

DROP GENERATION

Inkjet Printing Technology

There are two different mechanisms by which inkjet printers generate droplets, and these are generically known as continuous inkjet (CIJ) printing and drop-on-demand (DOD) inkjet printing (11). Both methods of drop generation can produce fluid drops with diameters in the range of 10 to 150 μm: CIJ printing is used mostly for coding and marking applications with a drop diameter of approximately 100 μm; DOD printing is dominant in graphics and text printing with a smaller drop diameter, typically 20–50 μm.

In CIJ printing a stream of drops is formed by the Rayleigh instability of a liquid column that is ejected under pressure through a small nozzle. To direct and position these drops, the nozzle is held at a potential relative to ground, which imparts a small charge on each drop as it is formed. Individual drops in the stream are steered by applying a further potential to deflector plates. A schematic diagram of a CIJ printer is shown in **Figure 1**. Drop diameters are typically slightly larger than the nozzle diameter. It is normal practice to impose a small pressure fluctuation on the liquid behind the nozzle through a piezoelectric transducer, which is used to synchronize drop formation if multiple nozzles are operating in parallel.

CIJ printing, by definition, produces a continuous stream of liquid drops, even when no printing is required. Unwanted drops are deflected by the electric field to a gutter, and for many applications in product marking and graphics, the unused ink is recycled (**Figure 1**). For most applications in materials science, this recycling after exposure to the environment risks

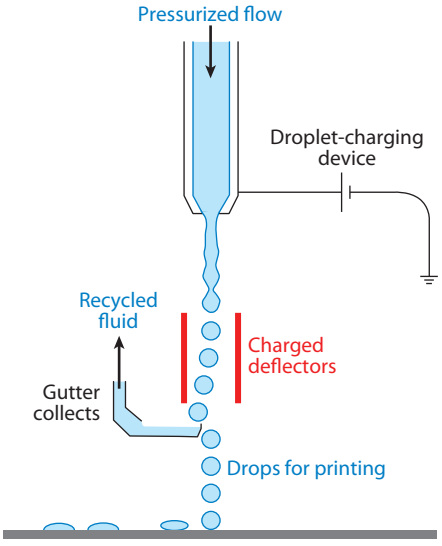

Figure 1

Schematic diagram showing the principles of operation of a continuous inkjet (CIJ) printer.

contamination of the ink; hence CIJ printing is a potentially wasteful process. Drop positioning is controlled either by steering a drop in flight or by positioning the substrate where a deposit is required and printing a drop. This second process is termed binary printing, as the drop is deposited into one of two locations, either on the substrate or in the recycling gutter. CIJ systems operate with drop generation rates in the region of 20–60 kHz, and drop velocity at the nozzle is typically >10 ms^{-1}.

DOD inkjet printers generate individual drops when required and are thus more economical with ink delivery than are CIJ systems. Drop positioning is achieved by manually locating the printer nozzle above the desired location on the substrate before drop ejection. Drops are formed by propagating a pressure pulse in the fluid held in a chamber behind the printing nozzle. If the pulse exceeds some threshold at the nozzle, a drop is ejected. In the absence of a pressure pulse, liquid is held in place by surface tension at the nozzle. It is normal to also control the static pressure at the nozzle to ensure that the meniscus at the nozzle is stable. In DOD systems, drops are generated at acoustic frequencies (typically 1–20 kHz), and resonances within the chamber behind the nozzle strongly influence pressure pulse propagation and drop generation (12, 13). Drop size is typically approximately equal to the nozzle size, but it is possible to control both drop size and ejection velocity (within a defined range) by management of the pressure pulse used to form the drops.

Two methods are used to generate the pressure pulse and to promote drop formation and ejection. In thermal DOD printing, a small thin-film heater is located in the fluid chamber. On passing a current through this heater, the fluid in immediate contact is heated to above its boiling temperature to form a small vapor pocket or bubble (**Figure 2*a***). After the current is removed, heat transfer leads to rapid bubble collapse. The rapid expansion and collapse of the bubble generate the required pressure pulse. In piezoelectric DOD printing, the pressure pulse is generated by direct mechanical actuation using a piezoelectric transducer (**Figure 2*b***). More recently, similar mechanical actuation has been achieved using MEMS technology and electrostatic forces.

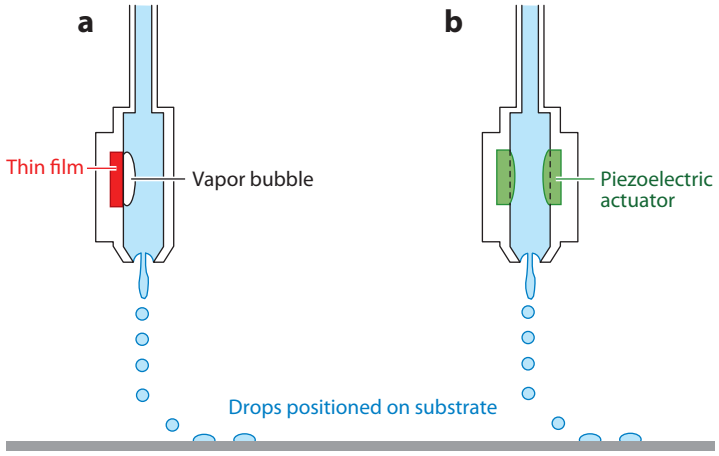

Figure 2

Schematic diagram showing the principles of operation of a drop-on-demand (DOD) inkjet printing system. Drops are ejected by a pressure pulse generated in a fluid-filled cavity behind the printing orifice. This pressure pulse can be generated by (*a*) a vapor pocket or bubble generated by a thin-film heater (thermal inkjet) or (*b*) a mechanical actuation, e.g., from a piezoelectric transducer (piezoelectric inkjet).

Figure 3 shows the sequence of drop formation observed at a DOD printer. The long extended fluid tail is a characteristic of the DOD process. The drop forms from an initial liquid column that thins to define a leading droplet and the elongated tail or ligament; the final rupture of the ligament can lead to the formation of satellite drops. Often these drops catch up and merge with the leading large drop in flight, prior to impact, in which case their presence is irrelevant. However, if they are still present at impact, they lead to noncircular impact footprints of the drop, with a deleterious influence on deposit precision, resolution, and accuracy. To facilitate drop merging in flight, it is customary to print at a stand-off distance from the substrate. For DOD printing this stand-off distance is typically 2–3 mm. The appropriate stand-off will also influence drop placement accuracy because drag from air currents in the printing environment can deviate drops from their desired trajectory. To minimize this effect, the stand-off distance is normally set at the minimum to ensure stable single drops.

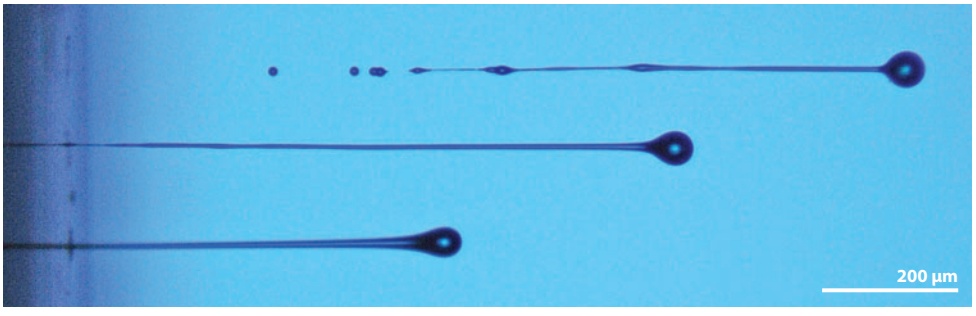

Figure 3

A high-speed photographic image showing three drops ejected from a DOD printer at different stages of drop formation. The drop forms from a single ejected liquid column that rapidly forms a leading drop followed by an elongated thin liquid tail. The tail breaks up into a trail of satellite droplets behind the primary drop. Reproduced with permission from Reference 11.

Thermal DOD systems are readily miniaturized, and most desktop or domestic printers use this technology. However, for two main reasons, the majority of industrial printers use piezoelectric DOD technology, and the majority of reports in the literature concerning inkjet printing of materials discuss using this method. First, the need to generate a bubble in thermal DOD printing limits the fluids to those of a high vapor pressure under ambient conditions. Second, with piezoelectric DOD printing it is relatively easy to change the actuation pulse to control drop size and velocity for any fluid. DOD printing operates at typical acoustic frequencies in the range of 1–20 kHz. Hence, given that the fluid-filled chambers used to generate drops have dimensions of the order of 10^{-3} m, significant acoustic resonances can influence drop volume and velocity (12, 13). Thus, the shape and amplitude of the actuating pulse can strongly influence printing behavior (11). Indeed, the design of an appropriate pulse to provide stable drop ejection conditions is regarded as critical know-how by manufacturers of inkjet printing equipment.

As discussed above, by far the majority of published work using inkjet technology for materials fabrication has reported using piezoelectric DOD printing. However, there has been significant work on thermal DOD printing as well. CIJ printing has been little used in materials science applications. This is partly because of the contamination/waste issue but also because a more limited range of fluids can be deposited using CIJ printing than is possible with DOD printing and because the spatial resolution of drops on the substrate is lower for CIJ printing than that achievable through DOD printing. However, CIJ printing has been used successfully to print 3-D ceramic objects (14) and silver conducting tracks (15). This review focuses on applications of DOD printing in materials science.

Printable Fluids

The generation of droplets in a DOD printer is a complex process, and the precise physics and fluid mechanics of the process are still the subject of much research (11). The behavior of liquid drops can be characterized by a number of dimensionless groupings of physical constants, the most useful of which are the Reynolds (*Re*), Weber (*We*), and Ohnesorge (*Oh*) numbers:

$$Re = \frac{v\rho a}{\eta}, \qquad 1a.$$

$$We = \frac{v^2\rho a}{\gamma}, \qquad 1b.$$

$$Oh = \frac{\sqrt{We}}{Re} = \frac{\eta}{(\gamma\rho a)^{1/2}}, \qquad 1c.$$

where ρ, η, and γ are the density, dynamic viscosity, and surface tension of the fluid respectively, v is the velocity, and a is a characteristic length.

The earliest significant work attempting to understand the mechanisms of drop generation was by Fromm (16). He identified the Ohnesorge number, *Oh*, as the appropriate grouping of physical constants to characterize drop formation. Confusingly, he used the parameter $Z = 1/Oh$ and proposed that $Z > 2$ for stable drop generation. This analysis was further refined by Reis & Derby (17), who used numerical simulation of drop formation to propose the following range, $10 > Z > 1$, for stable drop formation. At low values of Z, viscous dissipation prevents drop ejection, whereas at high values the primary drop is accompanied by a large number of satellite droplets.

Another limiting factor for drop generation is the influence of the fluid/air surface tension at the nozzle. A drop must have sufficient energy to overcome this barrier for ejection. Duineveld et al. (18) suggested that this leads to a minimum velocity for drop ejection of

$$v_{\min} = \left(\frac{4\gamma}{\rho d_n}\right)^{1/2}, \quad 2.$$

where d_n is the nozzle diameter. Equation 2 can be reformulated in terms of the Weber number to give a minimum value for printing,

$$We = v_{\min}\left(\frac{\rho d_n}{\lambda}\right)^{1/2} > 4. \quad 3.$$

Equation 3 does not include the influence of inertia but is a suitable value for benchmarking fluid properties.

Finally, we consider the impact of the ejected drop on a substrate. This process is considered in more detail below, but it is clear that the drop must impact so as to leave a single isolated spread drop. The appropriate threshold to consider here is that of splashing. The mechanisms that lead to the onset of splashing are also a topic of current research, but there is a well-established experimental threshold for the onset of splashing, first proposed by Stow & Hadfield (19) as a critical dimensionless grouping of variables:

$$We^{1/2}Re^{1/4} > f(R), \quad 4.$$

where $f(R)$ is a function of surface roughness only. This relationship has been explored by a number of authors, and for flat, smooth surfaces $f(R) \approx 50$ (20).

Through the use of Equations 2–4 and the limiting values of $Z = 1/Oh$, it is possible to construct a map in a parameter space, with coordinates *Re* and *We*, that can be used to define fluid properties that are usable in DOD inkjet systems. This is shown in **Figure 4**. The validity of this predicted regime of printability has been explored for a large range of fluid properties with particle-filled systems, and the map offers a useful guide for fluid properties selection (21). Other aspects of drop ejection from DOD printers scale with dimensionless groupings of physical properties. Reis et al. (13) found that the volume of an ejected drop scales with the Ohnesorge number and with the displacement of the actuation used to initiate drop ejection. Because of the effect of acoustic resonances, the speed of sound in the fluid is also important in controlling printed drop characteristics (22).

Up to this point, we have assumed that the fluid behaves in a linear Newtonian manner. However, for many applications in materials science, it is necessary to print polymer solutions or concentrated dispersions of particles. The rheological properties of such fluids can be highly nonlinear, and thus the printability characteristics of a fluid as displayed in **Figure 4** may need to be further modified. Haskal et al. (23) reported that for solutions of poly(*p*-phenylene vinylene) (PPV), the characteristic fluid tail that forms during DOD printing becomes longer and more stable. For 0.5–2.0% solutions in a range of solvents, the filament did not detach, and no individual drops were formed at molecular weights above 300 kDa (23). Similar behavior has been reported with a number of other polymer solutions, with extended and stable ligaments found with increasing polymer molecular weight and concentration. Xu et al. (24) explored the effect of concentration and molecular weight on printed drop behavior and concluded that the transition from a nearly Newtonian behavior to one dominated by fluid extensional elasticity can be explained in terms of conventional models of polymer solution behavior. Xu et al. also commented on the beneficial aspects of low polymer concentrations. Newtonian fluids show elongated tails

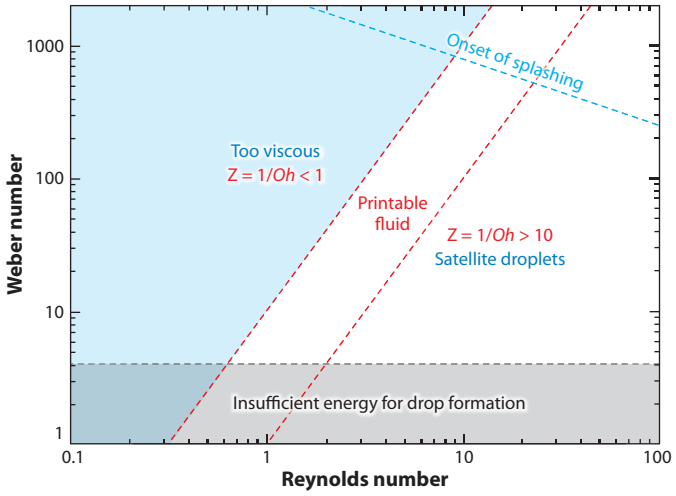

Figure 4

Equations 2–4, together with the range of $Z = 1/Oh$ that allows stable printing, can be plotted in a coordinate system defined by the Reynolds and Weber numbers to illustrate the regime of fluid properties where DOD inkjet printing is possible.

during DOD printing, and these can destabilize into a train of satellite droplets that follow the main drop (**Figure 3**). The action of small concentrations of polymers can stabilize the tail so that it retracts into the main drop during flight through surface tension, resulting in a single drop on impact.

DROP/SUBSTRATE INTERACTION

For most applications of interest to materials scientists, the liquid drop will impact on a substrate, and a subsequent phase change will transform the liquid into a solid. For some applications, this phase change will generate the final desired product, whereas for others a secondary process (e.g., sintering) is required. The liquid/solid phase change can occur by a number of mechanisms, including solvent evaporation, cooling through a transition temperature, gelling of a polymer precursor, and chemical reaction. In all these cases, solidification occurs postdeposition, and the printed pattern must retain some stability in the liquid state prior to solidification. To fully understand the processes that occur between the printed drop and the substrate prior to attaining the desired structure, we must identify the interactions that occur between the substrate and the fluid drop prior to solidification.

Drop Impact and Spreading

The behavior of a liquid drop on impacting a solid surface is controlled by a number of physical processes and can be driven by inertial forces, capillary forces, and gravitational forces. The important dimensionless groupings are the Reynolds, Weber, and Ohnesorge numbers, as with

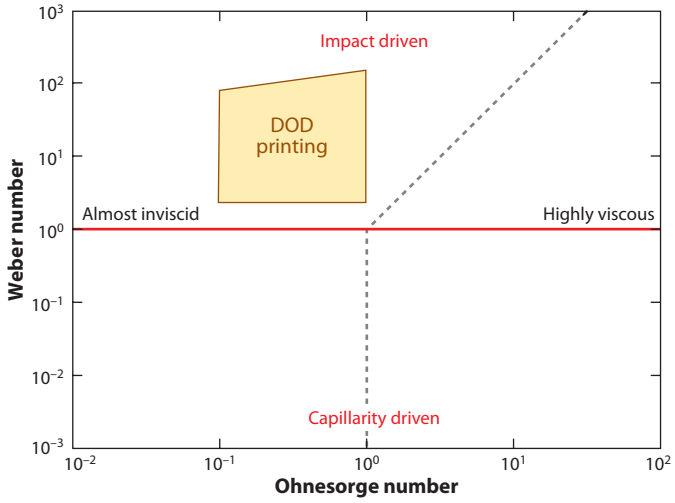

Figure 5

Parameter space defined by axes of Ohnesorge and Weber numbers showing the driving force for initial drop spreading after impact. The conditions for DOD inkjet printing (taken from **Figure 4**) are shaded, indicating that initial drop behavior is described by inertial or impact forces. Drawn following the schematic diagram of Schiaffino & Sonin (25).

drop generation, but we must also consider the Bond number, $Bo = \rho g a^2/\gamma$, where g is the acceleration of gravity when gravitational forces are included. Typical fluids used for inkjet printing have a density close to 1000 kg m^{-3} and a surface energy below 0.1 J m^{-2}, and in DOD printing the drops have diameters <100 μm. At these small length scales, $Bo \ll 1$; hence gravitational forces can be neglected. Thus, the dominant forces will be inertial and capillary. Schiaffino & Sonin (25) considered the impact of relatively low Weber number drops on a solid surface. Although their analysis was for solidifying drops, the initial stages after drop impact should be the same for all impacting fluids. They proposed that drop behavior on impact can be divided into two regimes: impact driven, in which the inertial forces dominate, and capillarity driven, in which initial drop velocity is unimportant and the transition in behavior occurs at a critical value of the Weber number. In addition, these authors characterized the resistance to spreading in terms of the Ohnesorge number, defining regimes as almost inviscous and highly viscous. **Figure 5** shows these researchers' representation of the regimes of initial impacting drop behavior, superimposed onto which is the regime of stable DOD drop formation taken from **Figure 4**. We can see that the initial stage of the interaction between an inkjet-printed drop and a substrate is impact driven in a region of relatively inviscous behavior.

Yarin (26) reviewed the behavior of impacting liquid drops in the velocity range 1–30 ms^{-1} and size range 100–3000 μm; this is sufficiently close to the regime of inkjet printing to provide a useful reference. Drop impact behavior can be conveniently divided into a number of timescales determined by the dimensionless time after impact, $t^* = t(v/d_0)$, where d_0 is the droplet diameter and v is droplet velocity (27). The initial impact stage is governed by kinematic behavior and has a duration of approximately $t^* = 0.1$ (or <1 μs for the dimensions and velocities appropriate for inkjet printing). This is followed by impact-driven spreading, recoil, and oscillation. At small values of t^*, viscous forces damp the spreading and oscillations, and surface tension forces become more important in controlling behavior. At later stages the capillary forces begin to dominate until, at $t^* \approx 10$–100 (0.1–1 ms), spreading is fully controlled by capillarity, and further extension

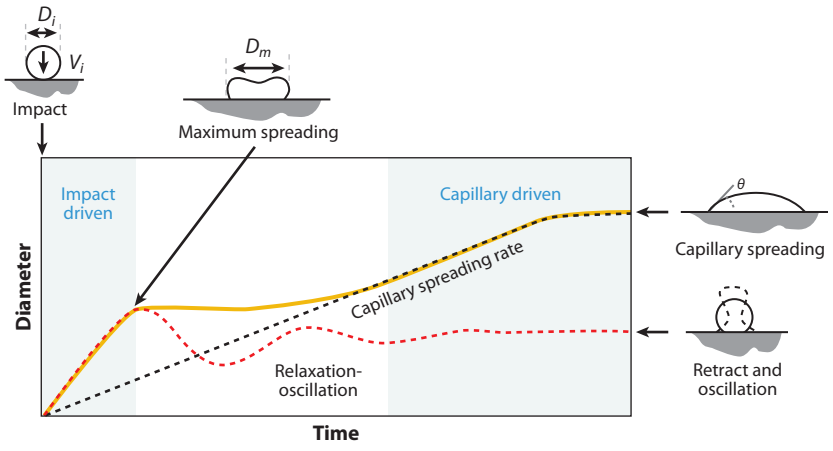

Figure 6

Schematic illustration of the sequence of events that occurs after droplet impact on a substrate. Initial impact is followed by a series of damped oscillations before capillary-driven flow occurs. θ is the contact angle, D_i is the initial droplet diameter, D_m is the maximum radius to which a droplet spreads during impact, and V_i is the droplet velocity at impact. Adapted from illustration provided by Dr. H.K. Hsiao, Institute of Manufacturing, University of Cambridge, United Kingdom.

occurs proportional to $t^{1/10}$ (28). Spreading continues and approaches true equilibrium at $t^* > 1000$. The sequence of these processes is illustrated schematically in **Figure 6**.

The final spread drop will have a contact diameter or footprint, d_{con}, determined by its volume and the equilibrium contact angle, θ_{eqm}. For drop sizes typical of inkjet printing, the Bond number is sufficiently small that the spread drop shape can be taken as a segment of a sphere, with

$$d_{con} = d_0 \sqrt[3]{\frac{8}{\tan\frac{\theta_{eqm}}{2}\left(3+\tan^2\frac{\theta_{eqm}}{2}\right)}}. \qquad 5.$$

Thus, the resolution, or minimum feature size of an inkjet-printed pattern, is controlled by the dimensions of this footprint, which is a linear function of the diameter of the drop in flight. The drop footprint increases with decreasing contact angle and is approximately $3d_0$ at a contact angle of 10°.

The contact angle is very important in controlling the final shape of a printed drop and patterns built up from the interaction of drops. As a drop spreads after impact, it advances over a dry surface, in which case the appropriate contact angle in Equation 5 is the static advancing contact angle rather than a true equilibrium value. However, in the production of patterns, drops may contact and interact with other drops. This interaction may lead to flow reversals, and in such cases the receding contact angle becomes important. Receding contact angles are also important if drop solidification occurs by solvent evaporation, in which case decreasing drop volume would be expected to lead to the drop footprint decreasing in area. However, drying droplets of solutions (especially polymer solutions) often show contact line pinning from solute deposition; this, combined with increased solvent evaporation rate toward the edge of the droplet, can lead to solute deposition in a ring at the contact line. This phenomenon is known as the coffee stain effect (29), which we discuss in more detail below. When contact line pinning occurs, the receding contact angle will decrease during evaporation and will tend toward zero.

Drop Coalescence and Pattern Stability

Conventional graphics printing requires patterns made up of isolated drops to produce a pixilated image. A key distinguishing feature between materials printing and graphics printing is that for many materials applications we require the drops to overlap to form continuous features. Thus, a key behavior is the interaction of spread or spreading droplets on a substrate to form stable liquid beads or lines and more complex 2-D patterns. 3-D structures are produced by overprinting sequential layers, but in this case a drop interacts with a solidified deposit and behaves in qualitatively the same manner as deposition on a substrate.

Davis (30) considered the stability of a fluid line or liquid bead on a flat surface subject to the following limiting conditions: (*a*) The contact angle at the line is fixed, and the contact line is free to move, (*b*) the contact angle is a function of the moving contact line speed with a limiting value at zero line speed, and (*c*) the contact angle is free to change, but the contact line is fixed. For cases *a* and *b*, the liquid bead undergoes a Rayleigh instability, but for case *c*, the liquid bead is stable if the contact angle is $<\pi/2$. Schiaffino & Sonin (31) studied these predictions experimentally and confirmed Davis's work.

Inkjet printing forms liquid beads through the overlap of adjacent spread drops. If there is no overlap of drops, there is no mechanism for the formation of liquid beads. Two overlapping drops will tend to coalesce, and a train of overlapping drops will form a bead, if there is significant contact line pinning. A number of authors have studied the behavior of overlapping drops and their transformation into liquid beads. Duineveld (32) investigated the behavior of inkjet-printed liquid drops on a range of substrates with different contact angles and found three regimes of behavior. When a liquid shows a constant contact angle (identical or very similar advancing and receding contact angles), the line is unstable, as predicted by Davis (30) and observed by Schiaffino & Sonin (31). If there is significant hysteresis in the contact angle, stable tracks can be printed at low values of the receding contact angle. However, even in this case it was not always possible to form a parallel liquid bead, and instead bulges were observed, spaced regularly along the printed liquid bead (**Figure 7**). The onset of this bulging instability is a function of both drop spacing and the speed at which the line was printed (i.e., the traversing velocity of the inkjet printer relative to the substrate). Duineveld (32) proposed a mechanism for this instability: It is caused by competition between possible flow paths when a newly deposited drop interacts with the leading edge of a liquid bead. If capillary spreading is relatively slow, the new drop at the front of a liquid bead will have a greater curvature at the liquid/air interface than the bead, and thus a difference in Laplace pressure will drive liquid from the front of the deposit along the preexisting bead. The transition in behavior occurs if the deposition flow rate (the number of drops arriving per second) exceeds the rate at which capillary spreading reduces drop curvature. Duineveld (32) developed this mechanism into a numerical model and predicted that the instability would occur at small droplet spacing and low traverse velocities (at constant drop generation rate); these predictions showed reasonable agreement with experiment.

Duineveld's (32) observations indicate that there is a maximum stable liquid bead width achievable through inkjet printing. Smith et al. (33) considered how a stable liquid bead was formed through droplet overlap. At low Bond numbers, the liquid bead will have a section equivalent to the segment of a circle defined by the contact angle. The width of the bead, w, can be determined, assuming volume conservation, from the drop volume, drop spacing (p), and contact angle, with

$$w = \sqrt{\frac{2\pi d_0^3}{3p\left(\frac{\theta^*}{\sin^2\theta^*} - \frac{\cos\theta^*}{\sin\theta^*}\right)}}. \qquad 6.$$

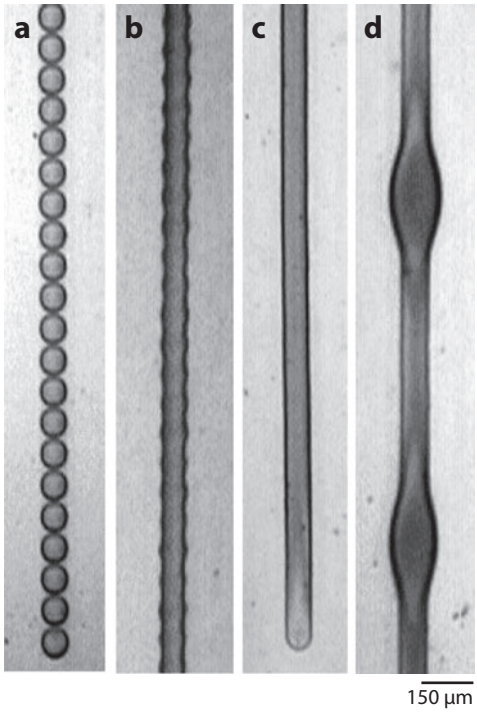

Figure 7

A liquid bead can form when a line of spread drops coalesce. (*a*) Drop spacing is too large for drop coalescence. (*b*) Initial coalescence leads to a liquid bead with a periodic irregularity. (*c*) After sufficient overlap a parallel-sided bead occurs. (*d*) If the drop spacing is too small, a bulging instability forms. The critical spacing is a function of the printhead traverse speed relative to the substrate. Figure adapted with permission from Reference 34. Copyright 2008, American Chemical Society.

In Equation 6 θ^* is the static advancing contact angle and not the equilibrium contact angle. Minimum line width will occur at the threshold for drop overlap, and as the drop spacing decreases, thicker liquid beads will form up to the threshold observed by Duineveld (32).

Soltman & Subramanian (34) carried out an experimental study of the formation of liquid beads from inkjet-printed drops. Their observations were consistent with those of both Duineveld (32) and Smith et al. (33). At large values of drop spacing, where no overlap of the spread drop footprint occurs, a train of discrete droplets is observed (**Figure 7*a***). At spacing slightly smaller than the diameter of the footprint, drop coalescence is observed, but the resulting liquid bead is "scalloped" and does not show parallel sides (**Figure 7*b***). At smaller deposited drop spacing, a stable liquid bead with smooth parallel sides is found (**Figure 7*c***), until finally the drop spacing is too small, and the bulging instability occurs (**Figure 7*d***). This work (34) demonstrated experimentally that there are two limiting lower and upper bounds to the width of a parallel-sided liquid bead produced by inkjet printing, even in the stability regime identified by Davis (30). Soltman & Subramanian (34) further commented on the fact that the instability proposed by Duineveld (32) was dynamic, and thus any consideration of the stability of inkjet-printed lines must take into account both printed drop spacing and the rate at which drops are deposited.

Stringer & Derby (35) demonstrated that it is possible to use the volume conservation model for liquid bead width (Equation 7) to define a lower bound for a stable liquid bead width. They

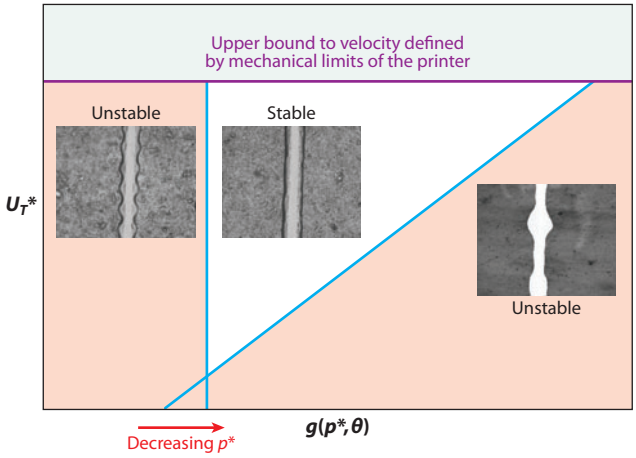

Figure 8

Stable, parallel-sided liquid beads are bound by two stability criteria, which can be represented in a parameter space bound by a function of the drop spacing and contact angle, $g(p^*, \theta)$, and a dimensionless printhead traverse velocity, $U_T{}^*$. For a given contact angle, there is a maximum droplet spacing above which the bead shows regular undulations [note that $g(p^*, \theta)$ is inversely related to the drop spacing]. There is also a minimum droplet spacing, which is a function of inkjet traverse speed, below which a dynamic instability leads to regular bulges on a continuous constant-width bead (36).

were also able to reformulate Duineveld's (32) model for the bulging instability in an analytical form. These two models can be used in combination to predict the limiting conditions (upper and lower bounds) under which inkjet printing produces stable liquid beads on a given substrate (36). These bounds are defined by three printing variables: the dimensionless drop spacing, $p^* = p/d_{con}$; the static advancing contact angle of the liquid on the substrate; and the traverse velocity of the inkjet printer nozzle relative to the substrate, U_T, made dimensionless through the relation $U_T^* = \eta U_T/\gamma$. This produces a simple diagram of the conditions for stable printing as shown in **Figure 8**.

In **Figure 8** the horizontal line at the top of the diagram represents the fact that, for any given printing system, there is a maximum traversing velocity for the printhead, and hence there is a practical upper bound to the stability diagram. The function $g(p^*, \theta)$ increases with decreasing value of the drop spacing. Thus, the vertical line to the left of the diagram defines the maximum drop spacing to produce a parallel-sided liquid bead or the minimum parallel-sided line width. The diagonal line defines the onset of the bulging instability at a critical minimum value of p^*, which is a function of the printhead traversing velocity and defines the maximum attainable line width. The physical value of the line width can be determined from any value of p^* by using Equation 6. The function $g(p^*, \theta)$ is such that the diagonal line is invariant with the contact angle but the vertical line is a function of the contact angle and moves to the left as θ decreases. Thus, Stringer's model predicts that lower contact angle fluid/substrate combinations show a larger range of droplet spacing for stable contact lines (36).

Patterned and Textured Substrates

On a smooth homogeneous surface, the resolution attainable from an inkjet printer is controlled by the diameter of the spread droplet or its footprint, which is a function of initial drop size and contact angle (Equation 5). Given that the smallest drops attainable from the current generation

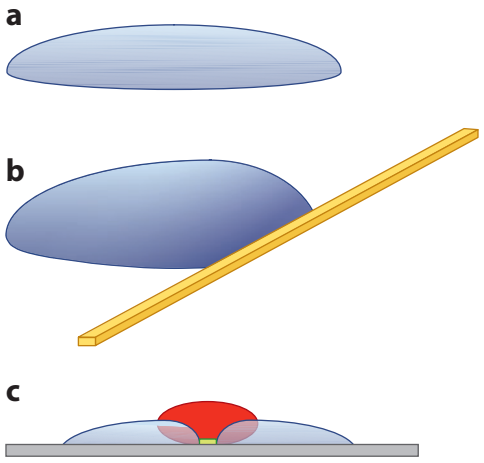

Figure 9

Fabrication of architectures by inkjet printing with dimensions smaller than a spread drop. (*a*) A droplet spread to its equilibrium configuration on a substrate. (*b*) The presence of a fluidphobic stripe (*yellow*) will arrest spreading. (*c*) A combination of two arrested drops defines the channel width between the source and drain beneath the gate for an all-polymer printed transistor (3). The red and green regions depict an organic polymer semiconductor and a gate-insulating layer respectively, deposited between the printed source, drain, and gate drops.

of DOD printers have a volume of ≈1 picoliter, or $d_0 > 10$ μm, the smallest feature size with a fluid of contact angle <10° will be >30 μm. For many applications in printed electronics, higher resolutions are required. To achieve this objective, the fluid flow during the spreading process is directed or restricted either by presenting a physical barrier to spreading by modifying the surface topology, or by patterning the substrate to locally control the surface energy and hence the contact angle of a spreading drop.

Sirringhaus et al. (3) were the first to use surface patterning to control substrate surface energies, and hence drop contact angles, prior to inkjet printing. They used photolithography and plasma etching of a polyimide film deposited on a glass substrate to produce a combined physical and surface energy barrier. This had a step height of ≈50 nm and an abrupt change in surface energy, giving a contact angle of approximately 20–25° on the exposed glass and approximately 70–80° on the polyimide. Using this pattern, they were able to produce linear channels with widths of ≈5 μm between overlapping printed drops of poly(3,4-ethylenedioxythiopene) doped with polystyrene sulfonic acid (PEDOT) (3), illustrated schematically in **Figure 9**. These structures were used to fabricate polymer transistors with channel widths of 5 μm, which is much smaller than the ≈80-μm footprint diameter expected from the inkjet-printed drops on their substrate. Wang et al. (37) demonstrated that it is possible to achieve similar- and smaller-width structures through dewetting, by printing a drop onto a fluidphobic stripe patterned on a fluidphilic substrate (**Figure 10*a–c***). By optimization of the mesa height, channel architectures with widths of ≈500 nm were achieved.

Another use of dewetting has allowed for channel architectures with dimensions of approximately 100 nm (38). In this method a PEDOT pattern is printed on glass, followed by a plasma surface treatment with CF_4 that decreases the PEDOT surface energy through fluoridation while increasing the surface energy of the glass. On printing a second PEDOT solution pattern, to overlap the original but modified PEDOT, the large contrast in surface energy dewets the

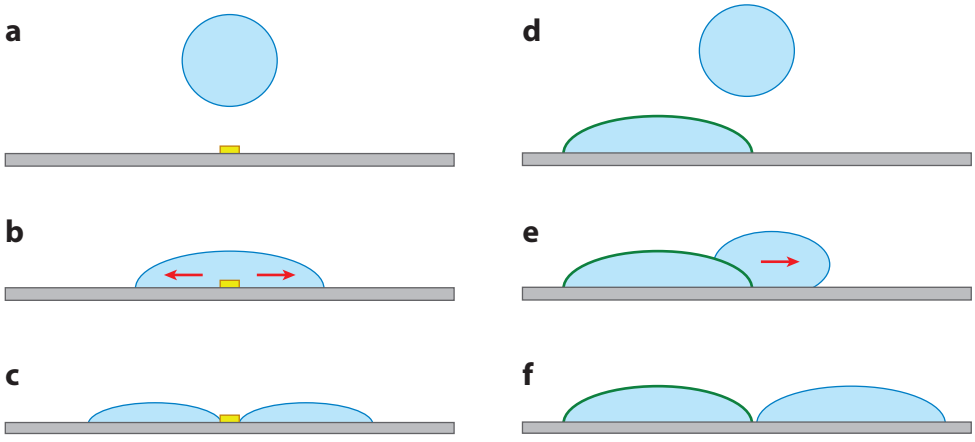

Figure 10

Fluid flow from dewetting can also be exploited to fabricate channels much smaller than drop dimensions. (*a*) A fluid drop is printed onto a fluidphilic substrate above a fluidphobic stripe (*yellow*). (*b*) Fluid flow within the drop is driven by dewetting energetics. (*c*) The final structure results in the fluid drop dividing into two drops separated by the narrow fluidphobic stripe. (*d*) A polystyrene sulfonic acid (PEDOT) solution drop is printed onto a solidified PEDOT structure that has been plasma treated to generate a fluidphobic surface (*green*). (*e*) The second drop is driven from the surface of the initial drop by dewetting; (*f*) two drops are separated by a narrow region after solidification. Subsequent processing to produce all-polymer transistors follows the schematic shown in **Figure 9*c***.

overlapping PEDOT. If the receding contact angle is not too small, no pinning occurs, and the resulting structure after drying is two adjacent PEDOT deposits separated by a small gap (**Figure 10*d*,*e***). These structures have been used to produce transistors for demonstration purposes. Further work has extended this process to polymer substrates (39).

Hendriks et al. (40) investigated the influence of grooved substrates produced by hot-embossing thermoplastic substrates. This work exploited the principle of capillary filling, in which fluids that show low contact angles will preferentially fill channels and textured surfaces (**Figure 11**) (41). Although this work has not explored the ultimate resolution of the method, lines with widths of ≈5 μm were produced with inkjet drops of diameter >100 μm. None of these methods that exploit topological or surface energy variation to direct the flow of fluids are immune to instability, particularly dynamic instabilities as reported by Duineveld (32) on planar surfaces. Pfohl et al. (41) discuss this and point out that if two liquid drops are connected by a microchannel, differences in Laplace pressure will drive fluid flow, the same driving force as modeled by Duineveld (32). Thus, although finer lines can be printed through this method than through simple droplet overlap on planar surfaces, other instabilities may remain.

Interactions with Porous Substrates and Drop Infiltration

An important application of inkjet printing in materials fabrication is the printing of a binder phase into a particle bed to fabricate 3-D objects (5). For this application there is a competition between spreading and infiltration processes as the drop impacts on the porous surface. These processes were studied by Holman et al. (42), who used a simple model for the infiltration of discrete fluid droplets developed by Denesuk et al. (43, 44). This model showed that, for droplets of the size produced by inkjet printing, infiltration times are in the range of 100–500 ms, which

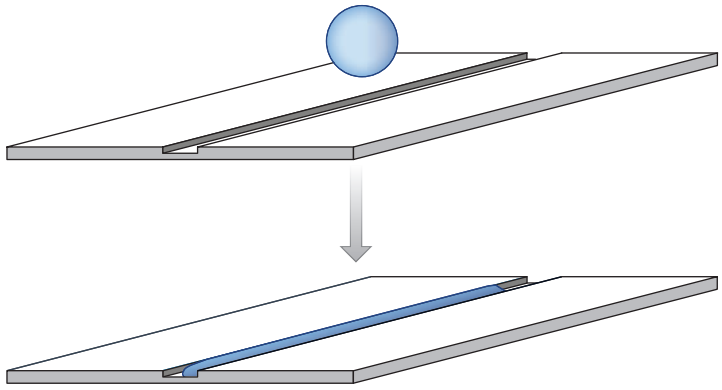

Figure 11

If a channel is cut or molded into a fluidphilic surface and subsequently a drop is deposited on the channel, the energetics of wetting will drive the fluid along the channel.

is significantly greater than the timescales for impact-driven and capillary spreading. Wang et al. (45) developed this analysis further by measuring the timescale for chemical reactions between an infiltrating fluid and a powder bed. These reactions occurred at still longer timescales, allowing the formation of solid objects by 3-D printing to be considered as three sequential processes of drop spreading, infiltration, and reaction (45).

Given the separation of the spreading and infiltration processes in the time domain, the above discussion on printed line stability and achievable resolution for printing liquid beads on planar substrates should apply to printing on powder beds.

DROP SOLIDIFICATION AND DEPOSIT SHAPE

The transition from a liquid deposit to the final desired solid material is the final step in the printing process. This transformation will almost always be accompanied by a reduction in volume. When solidification occurs by solute evaporation, the volume change may be particularly great because, to maintain viscosity within a regime suitable for printing, only dilute solutions of long-chain polymers and low volumes of particles in suspension are normally printable.

The mechanisms of solid formation through evaporation from a solution are of particular importance in a number of applications of inkjet printing of conducting and semiconducting polymers and also of printing of metal and ceramic nanoparticle suspensions. Solute distribution during drying can strongly influence the shape of a printed drop through the well-known coffee stain effect, when solute strongly segregates to the initial contact line (29, 46, 47). This phenomenon was explained by Deegan et al. (29), who observed that the rate of solvent evaporation is greatest toward the contact line because of easy vapor transport in the surrounding "dry" substrate. Thus, precipitation occurs first at the contact line. Because this deposit will pin the contact line, fluid flow will occur from the center of the drop to replace the evaporating fluid from close to the contact line. This peripheral flow continuously feeds the solidification at the contact line, and the final deposit will show a characteristic ring where the solute has segregated during the drying process. This phenomenon is important in controlling the shape of inkjet-printed drops and also occurs during the drying of liquid beads to result in a characteristic dual-ridged line profile after solidification (**Figure 12**).

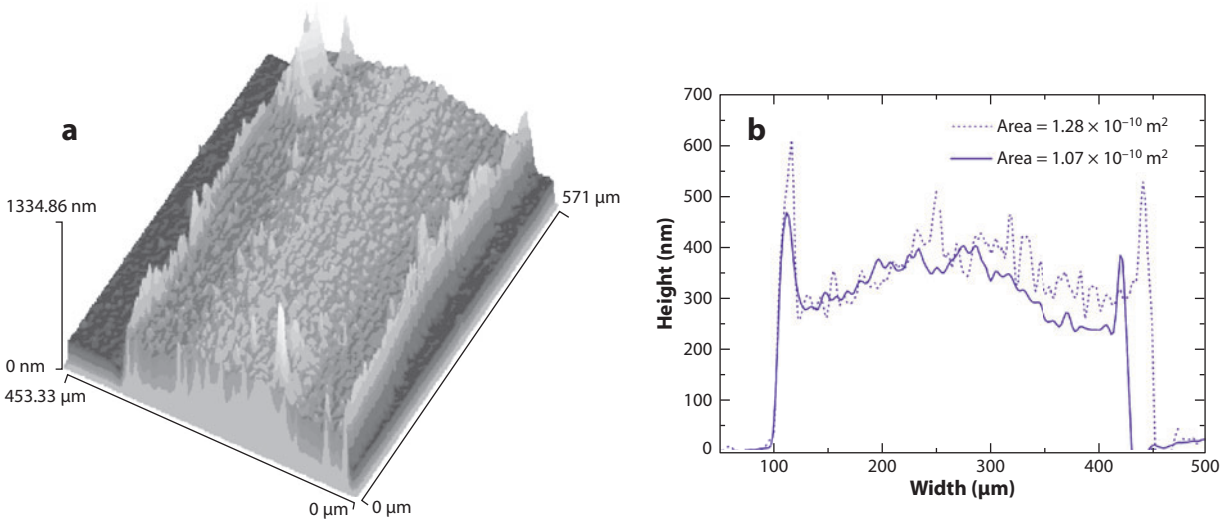

Figure 12

Observations of coffee staining from printed nanoparticle silver ink. (*a*) Interferometric image of a track formed from the drying of a liquid bead showing distinct ridges at the edges that have formed by fluid flow during drying. (*b*) Two line profiles across the track showing the variation in height across the track. Adapted from Reference 33.

Deegan et al. (29) solved for the evaporation flux of solvent as a function of radial distance r from the center of a droplet of contact radius R to find

$$J(r)\alpha(R-r)^{-\lambda} \qquad 7a.$$

with

$$\lambda = (\pi - 2\theta_{rec})/(2\pi - 2\theta_{rec}), \qquad 7b.$$

where θ_{rec} is the receding contact angle. For fluidphilic surfaces ($\theta_{rec} \ll \pi/2$), λ is positive, and thus the flux increases rapidly as we approach the drop edge or contact line. For the case of a pinned contact line, the resulting compensating outward flow of liquid increases as θ_{rec} decreases. Petsi & Burganos (48) solved Equations 7a and 7b for the case of a cylindrical section liquid bead and found a similar trend in flow behavior with contact angle.

Mechanisms to reduce coffee staining chiefly concern methods of modifying the driving force for fluid flow during the drying process. The enhanced evaporation at the edge of a spread drop occurs because of the large dry substrate surrounding it, which provides rapid vapor transport at the contact line. If the environment around the drying drop has an enhanced vapor pressure, both the difference in evaporation rates across the drop as well as the coffee stain will be reduced. However, this enhanced vapor pressure will reduce the overall drying rate of the deposit and may be difficult to engineer in practice. Soltman & Subramanian (34) observed that PEDOT solutions printed onto a cooled substrate show reduced coffee staining. Heat transfer through the drop is faster toward the edge of the drop, where the drop is thinner, generating a radial temperature profile with enhanced evaporation at the drop center to counter the evaporation at the drop edge. An alternative method to reduce coffee staining is to use a more complex solvent composition that contains fluids of different vapor pressures. The higher-vapor-pressure component will show a greater evaporation flux, which will set up radial concentration gradients in the drying drop. A suitable choice of fluids can be used to generate surface tension gradients that induce Marangoni

flows to counteract the evaporation-driven flow to the drop edge (49, 50). A final mechanism to reduce coffee staining is to impede fluid flow within the drop. Impedance can be easily achieved by inducing a phase change other than that through solvent depletion. Wax droplets filled with ceramic powders rapidly solidify on impact with a substrate, and no significant segregation of the solid has been seen (6, 51). Van Den Berg et al. (52) used a similar strategy, relying on a thermoreversible gel that solidified on impacting with a heated substrate. This ink displayed coffee staining after printing on a low-temperature substrate, but in a higher-temperature experiment coffee staining was eliminated by the fluid gelling rapidly, even though evaporation of solute occurred at a greater rate.

The majority of work on inkjet printing reported in the literature has concentrated on printing 2-D patterns, with limited 3-D capability through overprinting (e.g., for polymer semiconducting device fabrication). However, 3-D objects have been fabricated through inkjet printing for many years, not through the direct printing and solidification of fluids but through the printing of a binder phase onto a powder bed (5). Although commercially successful, printing onto a powder bed cannot be truly considered 3-D fabrication through inkjet printing, which we define as the fabrication of solid objects through the overprinting of liquid drops. A major limitation in 3-D printing has been the relatively low aspect ratio of a spread drop on a substrate, which after drying and solvent removal may have a height of <1 μm. Realistic 3-D printing of solid objects from ceramics has been achieved only with the development of highly fluid ceramic suspensions with very high solid loading (6, 50, 53–55). With 3-D printing, the requirement for accurate placement of drops is paramount to ensure that objects are efficiently built in the z direction. Evans and colleagues (55) have demonstrated very high aspect ratio features and thin-walled objects, but in doing so, the minimum feature width was defined by two drops, and thus a penalty of reduced x-y plane resolution was incurred.

FUTURE CHALLENGES

The challenge facing the use of inkjet printing for applications in advanced materials applications is feature resolution. The resolution of any printed object is clearly limited by the volume of the ejected drop. At present the limiting droplet size is approximately 1 picoliter, or a diameter of $\approx$12 μm. Although smaller liquid droplets can be generated by other technologies (e.g., electrostatic droplet ejection from a Taylor cone), it is unlikely that much smaller droplets will be available from inkjet printheads in the near future because of the limiting physics of the droplet generation process (11).

It is possible to achieve feature resolution higher than the drop size limit through patterning or structuring the substrate before printing (3, 37–40). However, the use of patterning effectively changes the advancing contact angle of the liquid. Moreover, as demonstrated by the initial work of Davis (30) and its development by Duineveld (32) and Stringer & Derby (36), the stability of a liquid bead is critically dependent on the behavior of the advancing and receding contact lines. These analyses of liquid line stability have been determined for planar homogeneous surfaces, and it is not clear that they are applicable to the stability of liquid beads confined by topographical or surface energy barriers. These prior studies have been simplified to make the problems tractable to analysis. New models need to be developed to identify the minimum feature size achievable through structuring. They should also consider the earlier impact-driven stages of drop/substrate interaction rather than just the capillary spreading stage. Such considerations are particularly important, as the splashing transition is a function of surface roughness (Equation 4) (19, 20). Thus, the interaction of impact-driven flow with structured surfaces must be studied.

The physics of drop drying is also of great importance in the manufacture of structures, with fluid flow and solute distribution strongly influenced by capillary and Marangoni flows (29, 49). In reality, drying phenomena are considerably more complex than the limiting condition modeled by Deegan et al. (29), with drying drops breaking free from pinning sites before repinning at a smaller contact line radius. Models of fluid flow during drying have to date chiefly considered simple symmetric structures (29, 46–48). Studies of drying droplets on structured surfaces where contact angles are controlled and/or fixed during evaporation would be a useful addition, considering the use of structured surfaces in determining pattern resolution. There are as yet no good models of the drying process that attempt to predict and include Marangoni flows that are formed through the evaporation of solvent mixtures. Such models would be very useful in predicting and controlling coffee staining and drying defects. Capillary forces can be considerable during the drying of nanoparticle suspensions, which can be exploited to structure deposits. For example, carbon nanotubes show strong orientation dependency on location within drying drops (56). Strong fluid flows are also expected when surface energy or surface topography patterning is used to define fluid location on a surface. The influence of these flows in concert with drying-induced flows needs further investigation, particularly if they are used to structure and to organize particle suspensions.

DISCLOSURE STATEMENT

The author is not aware of any affiliations, memberships, funding, or financial holdings that might be perceived as affecting the objectivity of this review.

ACKNOWLEDGMENTS

Much of the work covered in this review has been supported by the Engineering and Physical Sciences Research Council (EPSRC) through the following awards: GR/L42537/01, GR/L42551/01, GR/N13784/01, GR/N16969/01, GR/R64421/01, GR/T11920/01, and EP/D062128/1. Part of this study was also funded by the Office of Naval Research through contract N00014-03-1-0930. The author would like to acknowledge the following who have all contributed in part to the work reported: N. Reis, D.Y. Shin, P. Smith, J. Stringer, and A. Wallwork.

LITERATURE CITED

1. Williams C. 2006. Inkjet technology moves beyond paper. *Phys. World* 19:24–29
2. Bharathan J, Yang Y. 1998. Polymer electroluminescent devices processed by inkjet printing. I. Polymer light-emitting logo. *Appl. Phys. Lett.* 72:2660–62
3. Sirringhaus H, Kawase T, Friend RH, Shimoda T, Inbasekaran M, et al. 2000. High-resolution inkjet printing of all-polymer transistor circuits. *Science* 290:2123–26
4. Hayes DJ, Wallace DB, Cox WR. 1999. MicroJet printing of solder and polymers for multi-chip modules and chip-scale packages. *Proc. 1999 Int. Conf. High Density Packag. MCMs*, 3830:242–47. Denver, CO
5. Sachs E, Cima M, Williams P, Brancazio D, Cornie J. 1992. 3-Dimensional printing: rapid tooling and prototypes directly from a CAD model. *J. Eng. Ind. Trans. ASME* 114:481–88
6. Seerden KAM, Reis N, Evans JRG, Grant PS, Halloran JW, Derby B. 2001. Ink-jet printing of wax-based alumina suspensions. *J. Am. Ceram. Soc.* 84:2514–20
7. Setti L, Fraleoni-Morgera A, Ballarin B, Filippini A, Frascaro D, Piana C. 2005. An amperometric glucose biosensor prototype fabricated by thermal inkjet printing. *Biosens. Bioelectron.* 20:2019–26
8. Nakamura M, Kobayashi A, Takagi F, Watanabe A, Hiruma Y, et al. 2005. Biocompatible inkjet printing technique for designed seeding of individual living cells. *Tissue Eng.* 11:1658–66

9. Calvert P. 2001. Inkjet printing for materials and devices. *Chem. Mater.* 13:3299–305
10. de Gans BJ, Duineveld PC, Schubert US. 2004. Inkjet printing of polymers: state of the art and future developments. *Adv. Mater.* 16:203–13
11. Martin GD, Hoath SD, Hutchings IM. 2008. Inkjet printing: the physics of manipulating liquid jets and drops. *J. Phys. Conf. Ser.* 105:012001
12. Antohe BV, Wallace DB. 2002. Acoustic phenomena in a demand mode piezoelectric ink jet printer. *J. Imaging Sci. Technol.* 46:409–14
13. Reis N, Ainsley C, Derby B. 2005. Ink-jet delivery of particle suspensions by piezoelectric droplet ejectors. *J. Appl. Phys.* 97:094903
14. Blazdell PF, Evans JRG. 2000. Application of a continuous ink jet printer to solid freeforming of ceramics. *J. Mater. Process. Technol.* 99:94–102
15. Mei JF, Lovell MR, Mickle MH. 2005. Formulation and processing of novel conductive solution inks in continuous inkjet printing of 3-D electric circuits. *IEEE Trans. Electron. Packag. Manuf.* 28:265–73
16. Fromm JE. 1984. Numerical-calculation of the fluid-dynamics of drop-on-demand jets. *IBM J. Res. Dev.* 28:322–33
17. Reis N, Derby B. 2000. Ink jet deposition of ceramic suspensions: modelling and experiments of droplet formation. *MRS Symp. Proc.* 624:65–70
18. Duineveld PC, de Kok MA, Buechel M, Sempel AH, Mutsaers KAH, et al. 2001. Ink-jet printing of polymer light-emitting devices. *Proc. Conf. Org. Light-Emit. Mater. Devices V* 4464:59–67
19. Stow CD, Hadfield MG. 1981. An experimental investigation of fluid-flow resulting from the impact of a water drop with an unyielding dry surface. *Proc. R. Soc. London Ser. A* 373:419–41
20. Bhola R, Chandra S. 1999. Parameters controlling solidification of molten wax droplets falling on a solid surface. *J. Mater. Sci.* 34:4883–94
21. Derby B, Reis N. 2003. Inkjet printing of highly loaded particulate suspensions. *MRS Bull.* 28:815–18
22. Reis N, Ainsley C, Derby B. 2005. Viscosity and acoustic behavior of ceramic suspensions optimized for phase-change ink-jet printing. *J. Am. Ceram. Soc.* 88:802–8
23. Haskal EI, Buechel M, Dijksman JF, Duineveld PC, Meulenkamp EA, et al. 2002. Ink jet printing of passive-matrix polymer light emitting displays. *SID Symp. Dig. Tech. Pap.* 33:776–79
24. Xu D, Sanchez-Romaguera V, Barbosa S, Travis W, de Wit J, et al. 2007. Inkjet printing of polymer solutions and the role of chain entanglement. *J. Mater. Chem.* 17:4902–7
25. Schiaffino S, Sonin AA. 1997. Molten droplet deposition and solidification at low Weber numbers. *Phys. Fluids* 9:3172–87
26. Yarin AL. 2006. Drop impact dynamics: splashing, spreading, receding, bouncing. *Annu. Rev. Fluid Mech.* 38:159–92
27. Rioboo R, Marengo M, Tropea C. 2002. Time evolution of liquid drop impact onto solid, dry surfaces. *Exp. Fluids* 33:112–24
28. Tanner LH. 1979. Spreading of silicone oil droplets on horizontal surfaces. *J. Phys. D Appl. Phys.* 12:1473–84
29. Deegan RD, Bakajin O, Dupont TF, Huber G, Nagel SR, Witten TA. 1997. Capillary flow as the cause of ring stains from dried liquid drops. *Nature* 389:827–29
30. Davis SH. 1980. Moving contact lines and rivulet instabilities. 1. The static rivulet. *J. Fluid Mech.* 98:225–42
31. Schiaffino S, Sonin AA. 1997. Formation and stability of liquid and molten beads on a solid surface. *J. Fluid Mech.* 343:95–110
32. Duineveld PC. 2003. The stability of ink-jet printed lines of liquid with zero receding contact angle on a homogeneous substrate. *J. Fluid Mech.* 477:175–200
33. Smith PJ, Shin DY, Stringer JE, Derby B, Reis N. 2006. Direct ink-jet printing and low temperature conversion of conductive silver patterns. *J. Mater. Sci.* 41:4153–58
34. Soltman D, Subramanian V. 2008. Inkjet-printed line morphologies and temperature control of the coffee ring effect. *Langmuir* 24:2224–31
35. Stringer J, Derby B. 2009. Limits to feature size and resolution in inkjet printing. *J. Eur. Ceram. Soc.* 29:913–18

36. Stringer J, Derby B. 2010. The formation and stability of lines produced by inkjet printing. *Langmuir*. In press; doi:10.1021/1a101296e
37. Wang JZ, Zheng ZH, Li HW, Huck WTS, Sirringhaus H. 2004. Dewetting of conducting polymer inkjet droplets on patterned surfaces. *Nat. Mater.* 3:171–76
38. Sele CW, von Werne T, Friend RH, Sirringhaus H. 2005. Lithography-free, self-aligned inkjet printing with subhundred-nanometer resolution. *Adv. Mater.* 17:997–1001
39. Noh YY, Zhao N, Caironi M, Sirringhaus H. 2007. Downscaling of self-aligned, all-printed polymer thin-film transistors. *Nat. Nanotechnol.* 2:784–89. Erratum. 2008. *Nat. Nanotechnol.* 3:58
40. Hendriks CE, Smith PJ, Perelaer J, Van Den Berg AMJ, Schubert US. 2008. "Invisible" silver tracks produced by combining hot-embossing and inkjet printing. *Adv. Funct. Mater.* 18:1031–38
41. Pfohl T, Mugele F, Seemann R, Herminghaus S. 2003. Trends in microfluidics with complex fluids. *ChemPhysChem* 4:1291–98
42. Holman RK, Cima MJ, Uhland SA, Sachs E. 2002. Spreading and infiltration of inkjet-printed polymer solution droplets on a porous substrate. *J. Colloid Interface Sci.* 249:432–40
43. Denesuk M, Smith GL, Zelinski BJJ, Kreidl NJ, Uhlmann DR. 1993. Capillary penetration of liquid droplets into porous materials. *J. Colloid Interface Sci.* 158:114–20
44. Denesuk M, Zelinski BJJ, Kreidl NJ, Uhlmann DR. 1994. Dynamics of incomplete wetting on porous materials. *J. Colloid Interface Sci.* 168:142–51
45. Wang TM, Patel R, Derby B. 2008. Manufacture of 3-dimensional objects by reactive inkjet printing. *Soft Matter* 4:2513–18
46. Deegan RD, Bakajin O, Dupont TF, Huber G, Nagel SR, Witten TA. 2000. Contact line deposits in an evaporating drop. *Phys. Rev. E* 62:756–65
47. Deegan RD. 2000. Pattern formation in drying drops. *Phys. Rev. E* 61:475–85
48. Petsi AJ, Burganos VN. 2006. Evaporation-induced flow in an inviscid liquid line at any contact angle. *Phys. Rev. E* 73:9
49. de Gans BJ, Schubert US. 2004. Inkjet printing of well-defined polymer dots and arrays. *Langmuir* 20:7789–93
50. Zhang Y, Yang S, Chen L, Evans JRG. 2008. Shape changes during the drying of droplets of suspensions. *Langmuir* 24:3752–58
51. Smith P, Derby B, Reis N, Wallwork A, Ainsley C. 2004. Measured anisotropy of alumina components produced by direct ink-jet printing. *Key Eng. Mater. Euro Ceram. VIII* 264–268:693–96
52. Van Den Berg AMJ, de Laat AWM, Smith PJ, Perelaer J, Schubert US. 2007. Geometric control of inkjet printed features using a gelating polymer. *J. Mater. Chem.* 17:677–83
53. Lejeune M, Chartier T, Dossou-Yovo C, Noguera R. 2009. Ink-jet printing of ceramic micropillar arrays. *J. Eur. Ceram. Soc.* 29:905–11
54. Ainsley C, Reis N, Derby B. 2002. Freeform fabrication by controlled droplet deposition of powder filled melts. *J. Mater. Sci.* 37:3155–61
55. Zhao XL, Evans JRG, Edirisinghe MJ, Song JH. 2002. Direct ink-jet printing of vertical walls. *J. Am. Ceram. Soc.* 85:2113–15
56. Li QW, Zhu YT, Kinloch IA, Windle AH. 2006. Self-organization of carbon nanotubes in evaporating droplets. *J. Phys. Chem. B* 110:13926–30

Annual Review of
Materials Research

Volume 40, 2010

Contents